© Universiti Tun Hussein Onn Malaysia Publisher's Office

IJIE

Journal homepage: http://penerbit.uthm.edu.my/ojs/index.php/ijie
ISSN : 2229-838X e-ISSN : 2600-7916

The International Journal of Integrated Engineering

Monitoring of Deformation Behaviour of Unsaturated Soil Slope using Distributed Optical Fibre Sensor

Dayangku Salma Awang Ismail[1*], Azman Kassim[2]

[1]Faculty of Engineering,
Universiti Malaysia Sarawak, 94300 Kota Samarahan, Sarawak, MALAYSIA

[2]Faculty of Civil Engineering,
Universiti Teknologi Malaysia, 81310 Johor Bahru, Johor, MALAYSIA

*Corresponding Author

DOI: https://doi.org/10.30880/ijie.2020.12.09.024
Received 27 August 2020; Accepted 24 November 2020; Available online 30 December 2020

Abstract: A distributed optical fibre sensing system named Brillouin Optical Time Domain Analysis (BOTDA) is used to monitor the strain development of a laboratory soil slope model. The technology is yet to be fully implemented due to uncertainties of attachment method or the best way to set up optical fibre sensors for geo-structure health monitoring. The aim of study is to evaluate the deformation behaviour subjected to the development of horizontal strains from Brillouin-based optical fibre sensor of a residual soil slope under loading impact using BOTDA technology. In this study, a soil-embedded strain sensor placement approach was proposed to be installed in the 1g model of soil slope which was achieved via the horizontal planting of a three-layered optical fibre cable in S-curve forming slope. In this paper, however, only pilot tests result is demonstrated for preliminary data interpretation purposes. From the preliminary laboratory tests, the results show the soil-embedded sensing fibre arrangement has efficiently detected and measured the horizontal strain deformation due to loading. Therefore, it can be concluded that the sensing fibre was well-responded with the soil movement under loading impact.

Keywords: Monitoring, deformation behaviour, distributed optical fibre sensor, unsaturated soil slope

1. Introduction

The risk of slope failure could be carefully monitored through periodic soil movement. The development of different kind of monitoring instruments in the past few decades improve the soil displacement monitoring results such as inclinometer, tiltmeter, extensometer etc. The results were used to characterize site condition, verification of design assumptions, determining the effect of construction, impose the quality of workmanship and provide indicators to failures. Alternatively, optical fibre technology was introduced in geo-structure instrumentation monitoring including natural slopes or embankments due to unsusceptible nature of optical fibre sensor to electromagnetic fields, corrosion, moisture, or ageing [1]. The directly surface contact to soil slope sensors arrangement is still under uncertain evaluation due to the non-linear soil behaviour that influences the true strain deformation of the soil slope. In this study, the laboratory-sized slope test model used the distributed optical fibre sensor (DOFS) technology and the monitoring sensors were arranged directly contact on the soil slope. The sensors measured the horizontal strain deformation of an unsaturated soil slope soil mass when subjected to rainwater infiltration and surcharge load-induced failure. However, the paper is only limited to present the measured strain of optical fibre sensors resulted from load-induced failure of unsaturated soil slope from the preliminary tests of this project.

*Corresponding author: aidsalma@unimas.my

1.1 Principle of BOTDA

Fig. 1 demonstrates the three-dimensional mechanism of Brillouin gain spectrum for stimulated Brillouin signal for a BOTDA system. Brillouin optical time-domain analysis (BOTDA) has been introduced by Horiguchi and Tateda [2] as a novel measurement technique to monitor the attenuation of light pulse in optical fibre. BOTDA system is produced when two light waves; a weak continuous light wave or probe signal and the intensified pump pulse light wave in the opposite direction are coupled and frequency difference of Brillouin frequency shift between the light waves is then matched to the Brillouin frequency of optical fibre core which is dependent of strain and temperature variations [3]-[5]. The principle of stimulated scattering BOTDA sensing system depended on the energy interchanging process along the fibre cable length due to inhomogeneity of silica glass. The Brillouin scattering interaction had caused the process of amplification of the probing light signal owing to the transferred energy molecules from the pump light [6]. Hence, the intensification of the continuous probing signal can be measured as a function of time [7]. The aim of employing both pump and probe light signals is to magnify the Brillouin back-scattered stimulated signal which would be advantageous for a longer sensing distance compared to the spontaneous back-scattered signal from optical time-domain reflectometry (OTDR) system.

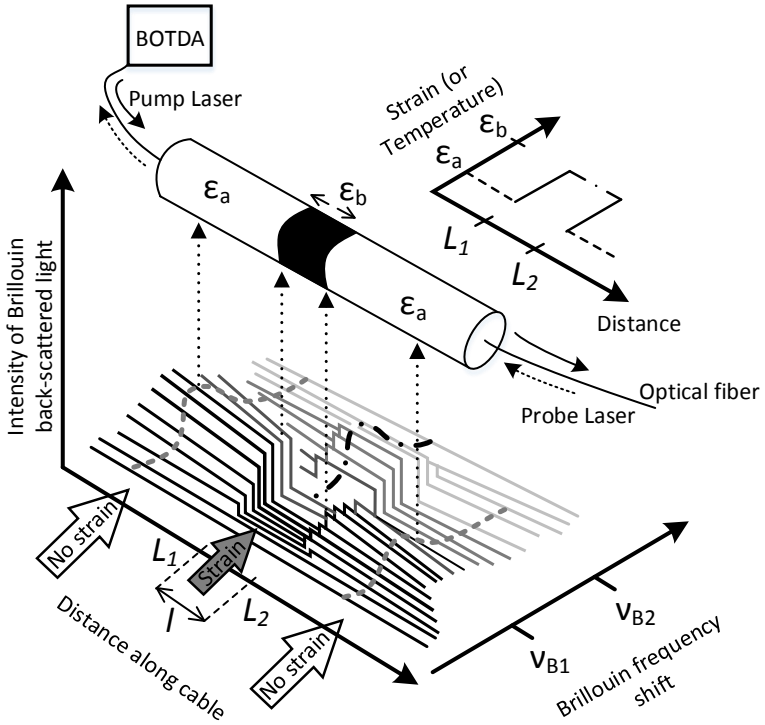

Fig.1 - The stimulated Brillouin gain is maximised when the frequency difference between pump and probe light equals to the local Brillouin frequency shift (BFS) [3]

2. Materials and Method

The laboratory modelling set up consisted of the construction of soil slope model, loading system, preparation of sensing fibre, the arrangement of soil-embedded fibre optic sensor, and close-range photogrammetry set up. The optical fibre sensors were arranged in three parallel segments behind the slope face and the computerized TML data logger was connected to the calibrated load cell for recording the raw data. The loading set up includes the pneumatic cylinder was also calibrated and the loading sequence was designed as a stress control system. The soil-water mixed was compacted into a series of horizontal soil layers and the compacted density was ensured to reach the desired suction value. The minimum matric suction targeted was about 26 kPa and the value was calculated from the mass-volume relationship formulas which associated the gravimetric and volumetric water content as specified in Eq. 1 [8], where θ is the volumetric water content, w is the gravimetric water content, ρ_d is the dry density of soil at w and ρ_w is the water density. The mini tensiometers' were then inserted into the soil slope model after the compaction procedure as to monitor if the acceptable suction measurement had reached the minimum value. The readings of the tensiometer should reach its minimum suction within 24 hours before testing commenced. Fig. 2 shows the limiting suction of 32 kPa selected as initial suction for the sandy silt for residual soil in UTM.

This value is defined as residual matric suction which are corresponded to residual water content, θ_r from soil water characteristic curve (SWCC). The limiting suction is theoretically understood to be achievable during its driest

condition. Previous studies in UTM (e.g. Gofar et al. [9], Lee et al. [10], Kassim [11]) had mentioned that the soil suction corresponding to residual water content in soil water characteristic curve is approximately equals to its dry condition. Nevertheless, the in-situ matric suction of residual soil was obtained at about 26 kPa during the driest condition at the similar area of study [11]. Therefore, the targeted controlled laboratory soil suction was acceptable within the range of 26 kPa to 32 kPa, which was the lower and upper bound of residual matric suction respectively.

$$\theta = w\frac{\rho_d}{\rho_w} \tag{1}$$

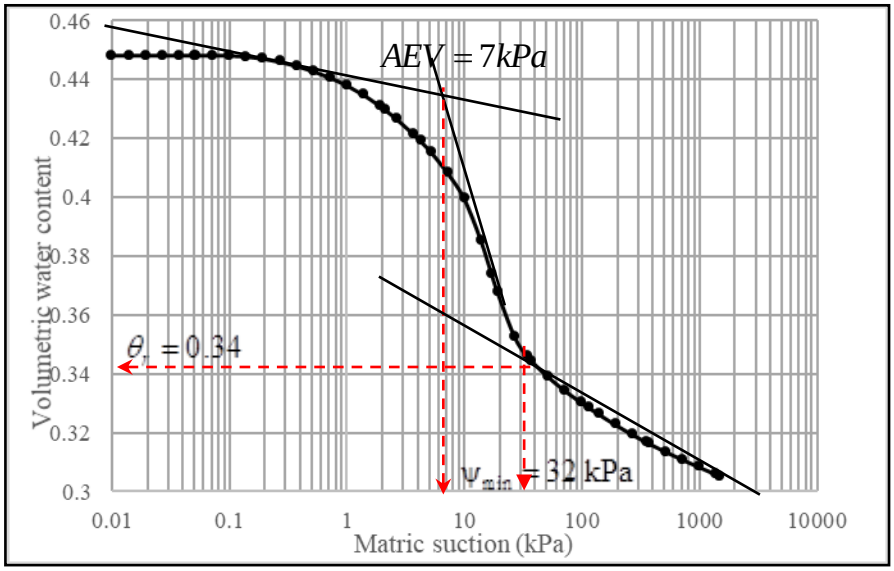

Fig.2 - SWCC curve for Grade V1 residual soil of this study

2.1 Instrumented Laboratory Model

Fig. 3 displays the finalized instrumented soil slope model for the physical modelling experiments. The figure shows the example of 27° soil slope model instrumented with tensiometers and optical fibre sensors. 14 mini tensiometers were installed along the pre-drilled sides of the Perspex chamber for suction measurement. The tensiometers were installed at three (3) different locations of the model slope; crest, middle and toe. The tensiometers were positioned at a similar distance which is at every 100 mm. The position of the tensiometers at each location were differed however, to suit the slope formation and numbers of datalogger's output channel. The tensiometers were then connected to the data acquisition system which consisted of Campbell Scientific Data Logger (Model CR10x, Campbell Scientific Inc.), a solid-state relay, and a desktop for data logging purposes. Optical fibre sensor was installed during the preparation of compacted sample behind the slope face to measure the soil strain deformation.

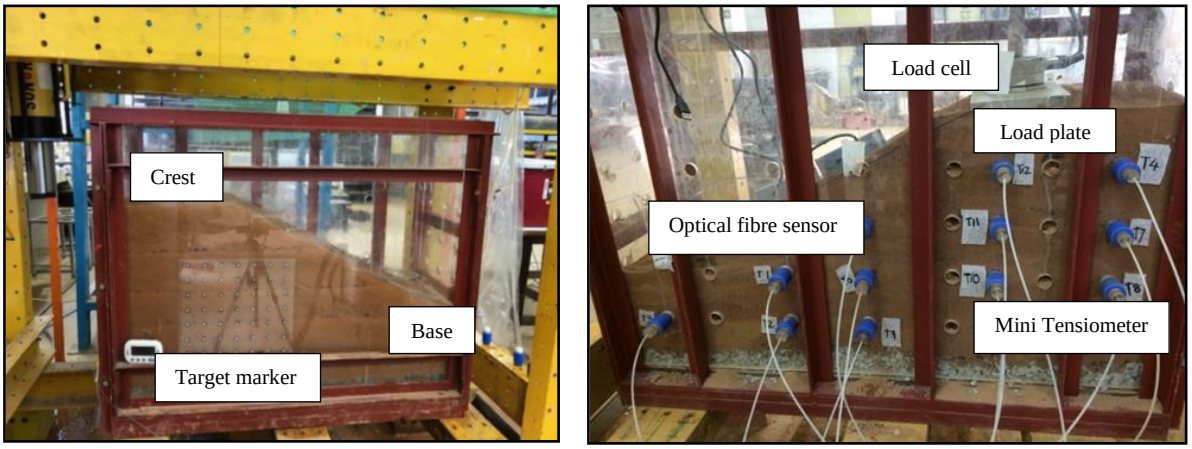

(a) (b)

Fig. 3 - (a) Instrumented soil model (Front side); (b) Instrumented soil model (Back side)

As illustrated in Fig. 4, each set of sensing fibre which laid at every compacted layer were installed in three parallel lines with notation A, B and C (refer to Fig. 3). The sensing fibres were installed at three different level of height behind the sloping face. The sensor cables were embedded inside the soil mass through one end insertion into the soil mass, arranged parallel to each other and followed by sandwiching the cables between layers of compacted soil. The first set of fibre optic sensor layout was installed after the 200 mm unsaturated soil compacted in the chamber. Each lines of sensing fibre was followed by a loose-state of 1-meter optical fibre that was not made contact to the soil movement. The sensing fibre outside of the chamber was purposely left to compensate for the temperature-strain effect and also used as spatial localization.

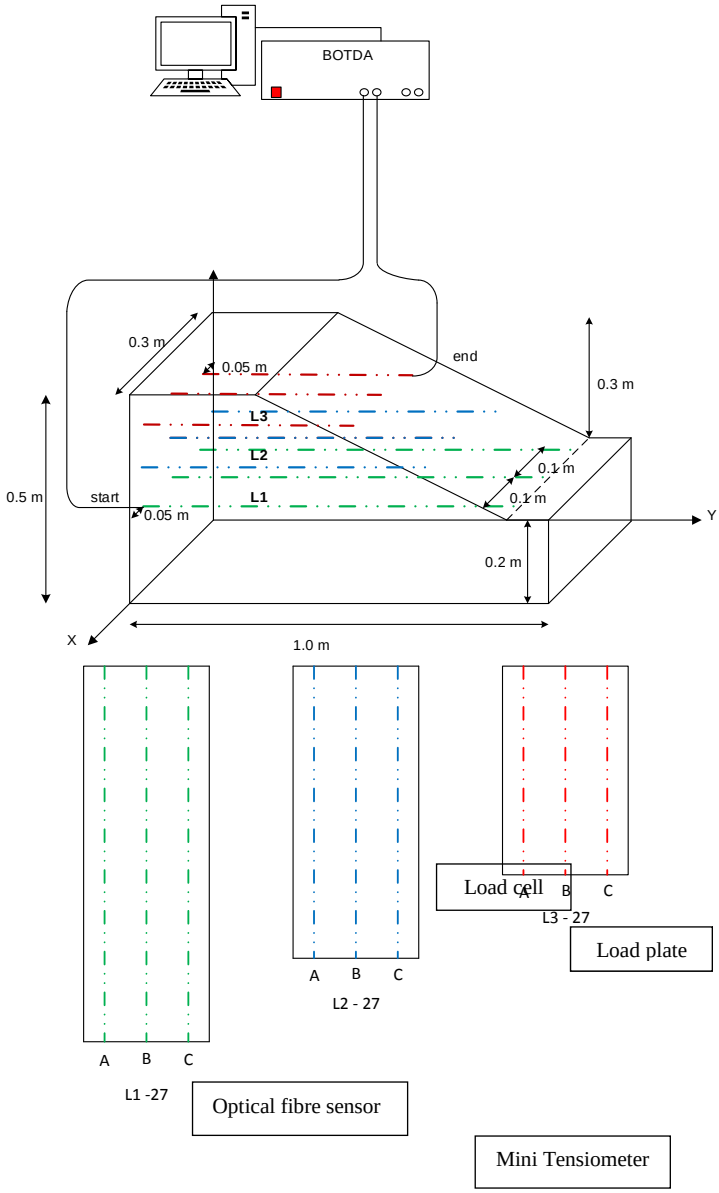

Fig. 4 - A diagram of sensing fibre arrangement (27° slope model)

Then, the second set of fibre optic sensor was laid on top of 100 mm compacted soil in an opposite direction of the previous sensor arrangement. The last set of embedded fibre optic sensor were laid and topped with 100 mm compacted soil. The first set of sensing fibre was referred to Layer 1 (L1) sensing fibre which at a distance of 300 mm from the crest. Then, the sensing fibre was positioned at 200 mm measured from crest and denoted as Layer 2 (L2). The uppermost layer which placed at 100 mm from the crest surface is labelled as Layer 3 (L3). The difference in length is due to the variability of slopes inclination angle. The parallel lines of A and C sensing fibre were laid about 50 mm from the wall chamber and Line B was installed at 150 mm distance from the wall chamber. Table 1 shows the variation of sensing fibre length for both slope angles; 27° and 45°. The fibre optic cables were connected to the BOTDA interrogator via dual channel; one end of the fibre optic cable were attached to Start channel and the other end

were connected to the End channels. Both ends of optical fibre were connected to the BOTDA interrogator unit via Angle Polished Connector (APC) fibre optic patch cords (Fig. 5) by inserting the cable to a hybrid adaptor or connector key, which equipped with the interrogator unit. The hybrid adaptor linked the sensor cable to the BOTDA interrogator. At the same time, images of the progressive failure process were also captured using DSLR camera. They were then analysed using Particle Image Velocimetry (PIV) method to process the captured images for comparison to the new optical fibre sensor instrumentation.

As for the loading apparatus, the surcharge loading equipment was comprised a loading frame, pressure controller, 10-bar CAMOZZI pneumatic cylinder, 20-tonne load cell and TML (JAPAN) 100mm Displacement Transducer. The incremental loadings were set-up in a stress-controlled manner. A pneumatic cylinder was connected to the 20-tonne load cell using 300mm fabricated iron-made connector. Conventional air pressure controller manually controlled uniform stress that transferred to 0.15m by 0.3m sized load plate. The steps of incremental load were observed through a computerized data acquisition system using TML (JAPAN) data logger. The load cell, pneumatic cylinder and the linear variable differential transformer (LVDT) were calibrated before any commencement of the test.

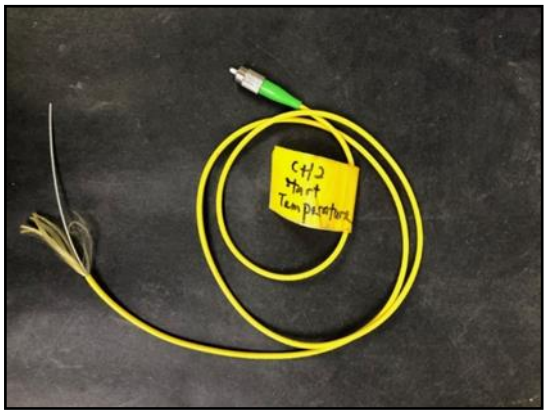

Fig. 5 - Angular patch cord (APC) connectors

Table 1 – Summary of the embedded length of optical fibre sensors

Slope	Layer	Optical fibre sensor in length (m)
27°	Layer 1A, B, C	0.9
	Layer 2A, B, C	0.7
	Layer 3A, B, C	0.5
45°	Layer 1A, B, C	0.6
	Layer 2A, B, C	0.5
	Layer 3A, B, C	0.4

3. Strain Data Measured from the Optical Fibre Sensor

The distributed optical fibre sensing system is known as ‘distributed’ due to obtaining the data in either strain, temperature or vibration along the fibre cables length over a certain gauge length with a small spacing reading. In general, DFOS system has several significant parameters which ideally represented the data such as spatial resolution, spatial step reading or read-out, measurement resolution, time of measurement and the sensing distance [12]. The measured strains of BOTDA are stated as the averaged value over its spatial resolution (0.5 m in this experimental programmes), and it is worth noting that it was challenging to locate maximum tensile strains when the strained length was lesser than the spatial resolution. The effect of spatial resolution on parameters settings for DOFS interrogator especially BOTDA is essential so that the measurements are correctly acquired and interpreted.

As for the preliminary results, the laboratory tests were named as S27R0P and S45R0P. The capital letter ‘S’ is denoted as slope angle in which two slope inclinations were considered; 27° and 45°. The subsequent letter ‘R’ were referred to rainfall intensity. The value is zero as no rainfall was involved in these laboratory schemes and the last letter which is P represented preliminary or pilot tests in the study. The unsaturated soil slope samples were regarded as the controlled samples and were forced to fail under incremental surcharge loading.

As mentioned in the previous section, the sensing fibres were laid in a longitudinal direction which were parallel to each other at three different layers behind the slope face which were denoted as Line A, B and C. Fig.6(a) and Fig. 6(b) illustrate the strain data development within a soil mass at layer 1 (L1) of the sensing fibre for 27° and 45°,

respectively. The three different curves were represented by the distribution of relative strain that acquired from the three parallel-arranged lines of sensing fibre. The peaks were understood as the maximum value of relative soil strain or displacement. For instance, Layer 1 (L1) of Test S27R0P produced three curves of strain data from the sensing fibre which each lines of sensing fibre equivalent to 0.9 m length (refer to Fig. 6(a)). The total length of sensing fibre at layer 1 (L1) is 4.7 m. The soil-embedded sensing fibre was started at the length of 5 m and ended at 9.7 m of the total length. The same installation procedure was performed for the 45° slope. Fig. 6(b) shows the distribution of strain of Test S45R0P. The length of L1 sensing fibre for the 45° slope was lesser than the former 27° slope. Since each lines (i.e A, B and C) of sensing fibre was only 0.6 m length, the total length of soil-embedded sensor would only about 3.8 m. The figure shows the soil-embedded fibre sensor is at the cable distance of 5 m to 8.8 m. A 1-m length of free-strained cable was reserved after each lines of embedded fibre cable to measure strain only due to the temperature change in the laboratory. As illustrated in Fig. 6, the maximum strain locations were found along the soil-embedded sensing fibre and Line B had shown the maximum strong amongst the lines. The distribution of soil strain for Line A and Line C of sensing fibre did replicate to each other due to similar arrangement in the chamber. From the pilot experiments, the strain distribution illustrates similar pattern regardless of slope inclination angle. In order to validate the feasibility of the proposed soil-embedded sensing fibre, the close range photogrammetry method was adopted to confirm the soil deformation behaviour.

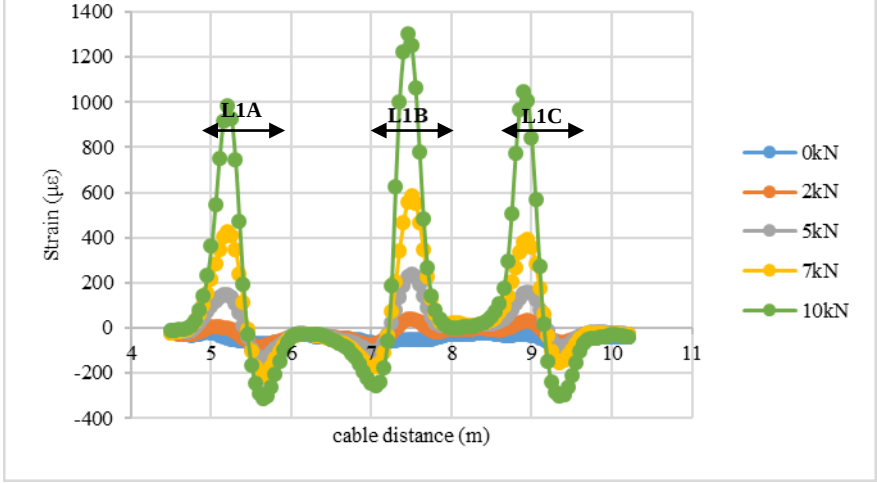

(a)

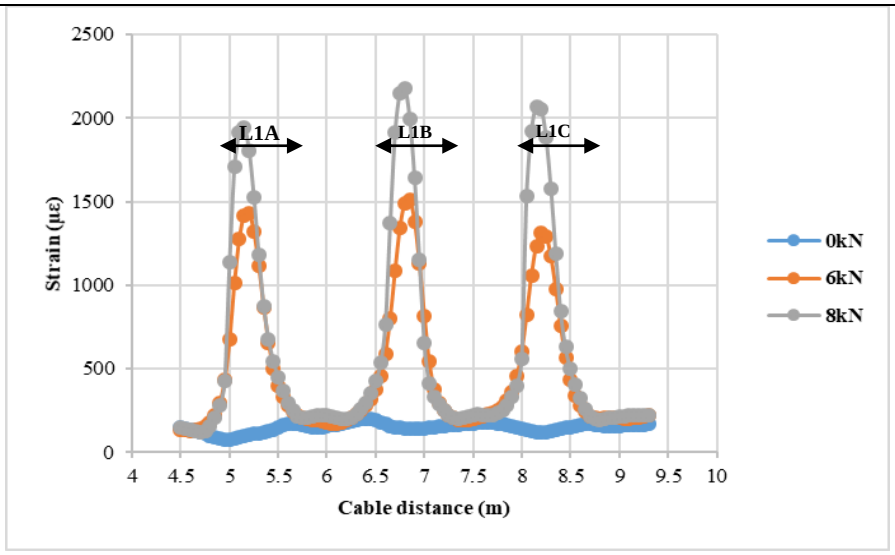

(b)

Fig.6 - Strain plot for Layer 1 (L1); (a) S27R0P and (b) S45R0P

The close-range photogrammetry is used to capture the images of testing and PIV method is latter used to detect the movement of the soil upon loading. Fig. 7 displays the shear strain contour which was calculations of the footing width and expressed in percentages. It was evident that the significant shear strain developed at the edges of the plate

and gradually reduce towards a deeper depth. The figure depicts the soil adjacent to and below the plate has been deformed about to 100% to 120% of the footing width which means the soil is failed. This observation was consistent with the ground movement pattern as described from the sensing fibre. As discussed earlier, the sensing fibres were horizontally placed at three levels; L3, L2 and L1 which are at the position from the upper to the lower level. The maximum axial strains first generated in upper layer L3 and followed by the subsequent lower level consistent with the load increment. The ground movement pattern depicts that the upper layer of the slope which was adjacent to the loading plate had failed and the relative strains measured at the particular layer (L3) had reached a constant value or reduction in which an indicator of failure for the respective soil layer (Fig. 8).

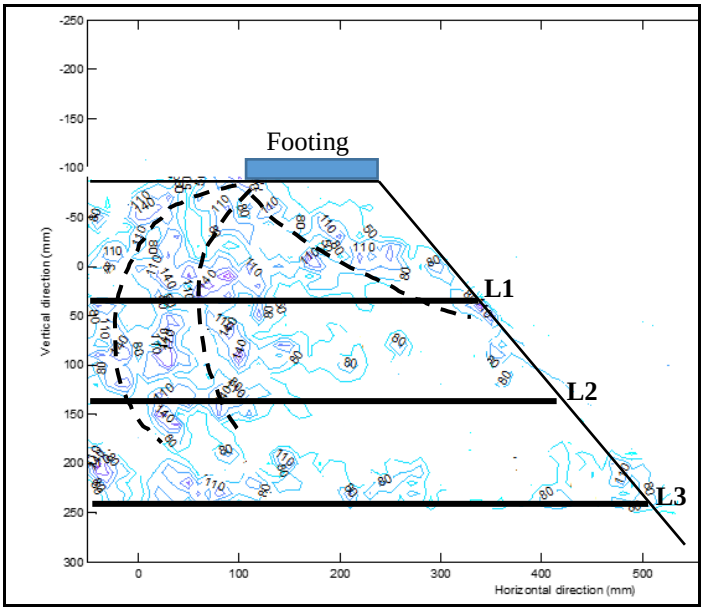

Fig.7 - PIV shear strain contour for S45R0P

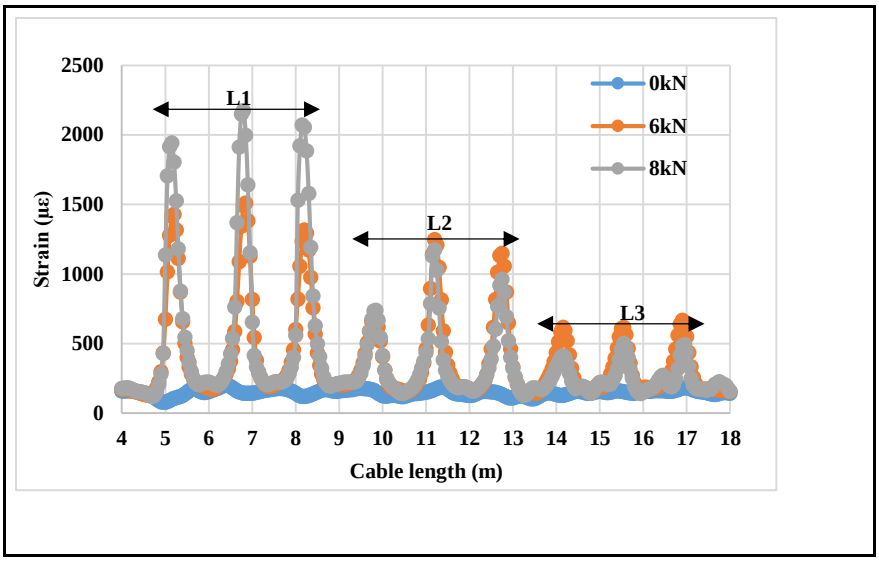

Fig. 8 - Strain distribution from the sensing fibre for S45R0P

Fig. 9 illustrates the soil slope model firstly collapsed due to the failure of the bearing capacity. The bearing capacity of a slope model is lower compared to the soil model with a horizontal surface because of the reduction of confining pressure due to the sloping side of a slope model. When the surcharge load is increased with time, the face of slope gradually collapsed because the mobilized shear stress from the resistance force provided by the self-weight of soil has reached the yield value of the soil shear strength. The result of sensing fibre at Layer 1 is regarded as relative soil deformation and the overall strain data from the test is replicating the soil behaviour of slope model when subjected to the excessive load on the footing. At the ultimate failure, the highest strain was perceived at Layer 1 with strain

reading about 2000 με. But the sensing fibre at Layer 2 and 3 denoted a sudden drop due to the ruptures of the soil-fibre bonded sensing system.

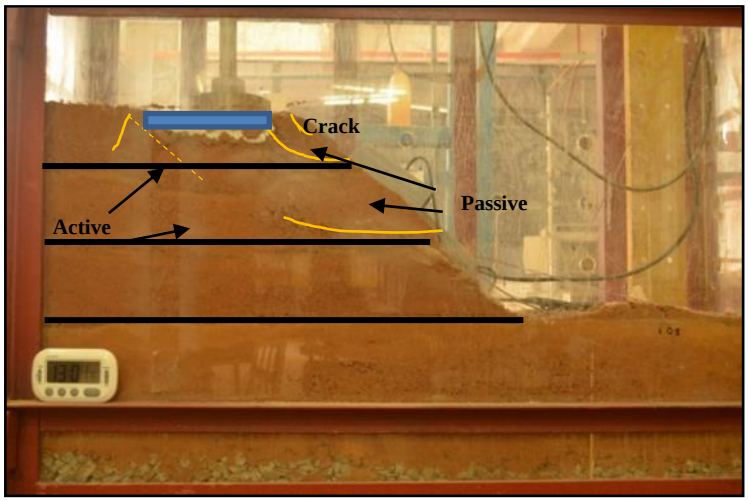

Fig.9 - Slope model at failure Test S45R0P

4. Conclusion

The preliminary laboratory modelling tests illustrated that the strain deformation owing to induced-load slope failure can be monitored using the embedded sensing fibre. This is because the design of embedded sensing fibre layout inside the soil slope model was sufficient to capture the progressive movement of the soil slope. Beforehand, the data acquisition system setting was involved for different parameter configuration to ensure the measure relative strain portrays the overall deformation of slope model. The tensile strain readings from the fibre optic sensors are signified the compressive behaviour of the soil particles. Therefore, it means when the soil is deformed in compression, the fibre optic sensor would react in tensile and vice versa.

Acknowledgement

The corresponding author would line to gratefully acknowledge the financial support provided by UNIMAS and Research University Grant (RUG) of UTM; Tier 1 Vote 11H04 which had made the research project workable.

References

[1] Mohamad, H. (2008) Distributed Optical Fibre Strain Sensing of Geotechnical Structures, Thesis. Cambridge University.
[2] Horiguchi, T. and Tateda, M. (1989). BOTDA—Nondestructive Measurement of Single-Mode Optical Fiber Attenuation Characteristics Using Brillouin Interaction: Theory, Journal of Lightwave Technology, 7(8), 1170–1176.
[3] Madjdabadi, B., Valley, B., Dusseault, M. B. and Kaiser, P. K. (2016). Experimental evaluation of a distributed Brillouin sensing system for measuring extensional and shear deformation in rock, Measurement: Journal of the International Measurement Confederation. Elsevier Ltd, 77, 54–66
[4] Hong, C. Y., Zhang, Y. F., Li, G. W., Zhang, M. X. and Liu, Z. X. (2017). Recent progress of using Brillouin distributed fiber optic sensors for geotechnical health monitoring, Sensors and Actuators, A: Physical. Elsevier B.V., 258, 131–145.
[5] Liu, J., Wang, Y., Lu, Y., Wei, J. and Kanungo, D. P. (2017). Application of distributed optical fiber sensing technique in monitoring the ground deformation, Journal of Sensors, 2017.
[6] Barrias, A., Casas, J. and Villalba, S. (2016). A Review of Distributed Optical Fiber Sensors for Civil Engineering Applications, Sensors, 16(5), p. 748.
[7] Iten, M. (2011). Novel Applications of Distributed Fiber- Optic Sensing in Geotechnical Engineering. ETH Zurich.
[8] Fredlund, D. G., Rahardjo, H. and Fredlund, M. D. (2012). Unsaturated Soil Mechanics in Engineering Practice. John Wiley & Sons, Inc.
[9] Gofar, N., Lee, L. M. and Kassim, A. (2008). Response of suction distribution to rainfall infiltration in soil slope, Electronic Journal of Geotechnical Engineering, 13 E(1999).

[10] Lee, L. M., Gofar, N. and Rahardjo, H. (2009). A simple model for preliminary evaluation of rainfall-induced slope instability, Engineering Geology. Elsevier B.V., 108(3–4), 272–285.
[11] Kassim, A. (2011). Modelling the Effect of Heterogeneities on Suction Distribution Behaviour in Tropical Residual Soil, Thesis. Universiti Teknologi Malaysia.
[12] Soga, K. and Luo, L. (2018). Distributed fiber optics sensors for civil engineering infrastructure sensing, Journal of Structural Integrity and Maintenance. Taylor & Francis, 3(1), 1–21.